IEEE Access
Multidisciplinary | Rapid Review | Open Access Journal

Received July 3, 2019, accepted July 15, 2019, date of publication July 24, 2019, date of current version August 9, 2019.

Digital Object Identifier 10.1109/ACCESS.2019.2930759

A New Geosynchronous SAR Constellation and Its Signal Characteristics

HAILONG XU[1,2,3], LIJIA HUANG[2,3], XIAOLAN QIU[2,3], (Senior Member, IEEE), BING HAN[2,3], LIHUA ZHONG[2,3], AND DADI MENG[2,3]

[1]School of Electronic, Electrical and Communication Engineering, University of Chinese Academy of Sciences, Beijing 100049, China
[2]Key Laboratory of Technology in Geo-Spatial Information Processing and Application System, Chinese Academy of Sciences, Beijing 100190, China
[3]Institute of Electronics, Chinese Academy of Sciences, Beijing 100190, China

Corresponding author: Lijia Huang (iecas8huanglijia@163.com)

This work was supported by the National Natural Science Foundation of China under Grant 60972149 and Grant 61101200.

ABSTRACT The Geosynchronous Synthetic Aperture Radar (GEO SAR) has a long synthetic aperture time. The temporal decoherence and azimuth variance characteristics of echo are significant, that brings great challenges to signal to process. In order to reduce the synthetic aperture time and thus improve the observation flexibility and efficiency, this paper proposes a SAR system mounted on a special satellite in reverse equatorial geosynchronous orbit, so-called the reverse equatorial GEO SAR. The orbit is nearly circular and the orbital plane coincides with the equatorial plane. The satellite flies against the direction of the Earth's rotation. The relative velocity is accelerated twice and the synthetic aperture time is shorter. The satellite does not drift in latitude direction and drifts uniformly in longitude direction. The echo has azimuth invariance property. Meanwhile, the 24-hour continuous observation can be achieved for areas with a certain range of latitude by means of large squint technique and constellation design. As the GEO SAR has high orbit, large delay, large squint angle, and wide pulse width, the complex modulation effects are generated by continuous motion between the satellite and target during the imaging period. In this paper, the uniform acceleration curve motion is used to describe the motion of both satellite and target, and the linear approximation is used to describe the slant range change in the process of transmitting and receiving one pulse. Accordingly, an accurate signal model for the reverse equatorial GEO SAR is established, which provides a theoretical model for signal characteristics analysis and imaging algorithms development.

INDEX TERMS Geosynchronous SAR, SAR constellation, SAR signal model.

I. INTRODUCTION

The satellite-based Synthetic Aperture Radar (SAR) is known as spaceborne SAR. Currently, the spaceborne SAR satellites are all in low-orbit. After years of development, the technology of low-orbit SAR has been relatively mature. However, due to the restriction of orbital height, the temporal resolution cannot be greatly improved. The geosynchronous (GEO) SAR, mounted on the geosynchronous satellite platform, has higher orbital altitude, larger field of view, shorter orbital period, and better temporal resolution [1], [2]. It is able to quickly revisit the fixed area and to continuously observe the fixed area for a long time [3]. Therefore, the GEO SAR has gradually become a research hotspot in the spaceborne SAR field [4]–[6].

The associate editor coordinating the review of this manuscript and approving it for publication was Prakasam Periasamy.

The resolution of spaceborne SAR is proportional to slant range and inversely proportional to relative velocity and synthetic aperture time. Therefore, the GEO SAR usually takes hundreds or even thousands of seconds of synthetic aperture time to achieve high resolution [7]. In that case, the variation of both radar system and target scattering characteristics will cause decoherence problems, which will affect the azimuth focusing ability of SAR [8]. In addition, the long synthetic aperture time will cause problems such as modeling of slant range histories and batch processing of azimuth variant signals, which will make the imaging algorithms more difficult [9], [10].

The spaceborne SAR generally adopts side looking geometry, so the observable orbit arc of target area is short. The use of large squint technology can extend the observable orbit arc to a great extent and increase the flexibility and efficiency of observation [11]. However, it leads to further increasement

of synthetic aperture time and still has imaging blind areas such as forward-looking, backward-looking and downward-looking areas. Therefore, it is impossible for a single GEO SAR satellite to achieve 24-hour continuous observation of a fixed area. The satellite network is a way to overcome this problem [12]. In [13], NASA and JPL proposed the global earthquake satellite system (GESS) program, which included five groups of satellites. Each group consists of two GEO SAR satellites with the same ground track of nadir point and 180 degrees apart in satellite's latitude angle. Each GEO SAR satellite runs on a circular orbit with an inclination of 60 degrees. The GESS constellation (abbreviated as ConI below) has nearly continuously global observation ability, but is faced to long synthetic aperture time, great difficulty in signal processing and big difference in global imaging performance.

To overcome these problems above, a new GEO SAR constellation (abbreviated as ConII below) is proposed in this paper. Firstly, the satellites are evenly distributed on a circular orbit that coincides with the equatorial plane. The angular velocity of the satellite is the same as that of the Earth, and the direction is opposite. It means that the satellite flies from east to west. In Earth-Centered Earth-Fixed (ECEF) coordinate, the angular velocity of the satellite is doubled and the synthetic aperture time is greatly shortened. A single GEO SAR adopts the large squint technology to observe a specific target area for a long time. When the acceptable squint angle range is exceeded, the latter GEO SAR takes the place of the current one to achieve 24-hour continuous observation. This GEO SAR ConII has exactly the same observation geometry for the surface with the same latitude and different longitude (Without considering the surface topography, the Earth is assumed to be an ellipsoid). The echo has invariant characteristic along azimuth direction, which greatly simplifies the imaging algorithms and maintains imaging performance consistency.

Due to the large squint angle and large propagation delay of the proposed GEO SAR, the radial velocity becomes larger, and the slant range changes faster. Thus, the assumption of stop-and-go gets invalid, which causes two effects [14]–[18]. One is the slow-time effect, which makes accurate calculation of two-way slant range difficult. The other is the fast-time effect, which modulates each pulse and makes the signal modeling complicated. References [16] and [17] take these two effects into account in airborne SAR geometry, where both the orbit bending and the Earth rotation are ignored. References [14], [15], [18], and [22] research in spaceborne SAR geometry. In [14], an ''equivalent position'' model is proposed to deal with the slow-time effect. In [22], a uniformly linear motion is used instead of stop-and-go to get the analytical expression of two-way slant range. Meanwhile, a simplified compensation for fast-time effect is given in azimuth time domain. In [15], the linear terms in azimuth frequency domain are compensated for fast-time effect, but the complete formation is not established and the effects of higher order terms cannot be revealed. In [18], a complete formation for compensation is carefully established, which is based on a modified hyperbolic rang equation (MHRE). MHRE approximates to the cubic terms of actual slant range precisely, but the quartic error cannot be ignored as the synthetic aperture time is very long in GEO SAR.

This paper establishes an analytical solution for two-way slant range calculation based on curvilinear motion of uniform acceleration of both satellite and target. Then, the linear approximation is carried out to describe the slant range changing over fast time within transmission and reception process of one pulse. Accordingly, the complete formation of GEO SAR echo is derived, which provides a precise model for signal characteristics analysis and imaging algorithms development.

The rest of this paper is organized as follows: Section II describes how to design the new GEO SAR constellation, and shows its advantages in mid-latitude observation by simulation results. Section III constructs the curvilinear motion of constant acceleration for satellite and target, and then derives the accurate slant range expression, the precision of which is validated by contrast with the other slant range expression. Section IV establishes the modified signal model in both time domain and frequency domain, in terms of the linear slant range variation within each pulse process. The simulation results verify that the modified signal model is effective in both side looking and squint looking geometries.

II. GEO SAR CONSTELLATION DESIGNING

The relative movement between the spaceborne SAR and the observed target is comprised of satellite orbital motion and Earth's rotation. If the included angle between two angular velocity vectors of satellite and Earth is below 90 degrees, the Earth's rotation cancels out the satellite motion to some extent. Otherwise, the relative motion is enhanced, and the synthetic aperture time is shortened. The imaging geometry changes a great deal over the orbit, that is the reason why the received echo shows azimuth variance property. As the orbital drift in latitude gets larger, the azimuth variety gets more serious, and vice versa. Based on the two points above, a new GEO SAR ConII flying in reverse equatorial plane is introduced in this section. The range and azimuth resolution expressions are deduced out to establish the SAR parameters. The controlling strategy of satellite platform and radar antenna is given to make the sensor footprint illuminate the target for a long time. The constellation is design to realize 24-hour continuous observation for mid-latitude region. At last, the performance of the proposed ConII is analyzed by comparing with ConI.

A. IMAGING TIME OF SINGLE GEO SAR

The single GEO SAR geometry in relation to a given target is shown in Fig. 1. Compared with the GEO SAR given in ConI, this new GEO SAR has the following characteristics: (1) During one orbital period, the satellite orbits the Earth twice and repeats the observation period for 12 hours; (2) The ground track of nadir point is always limited within

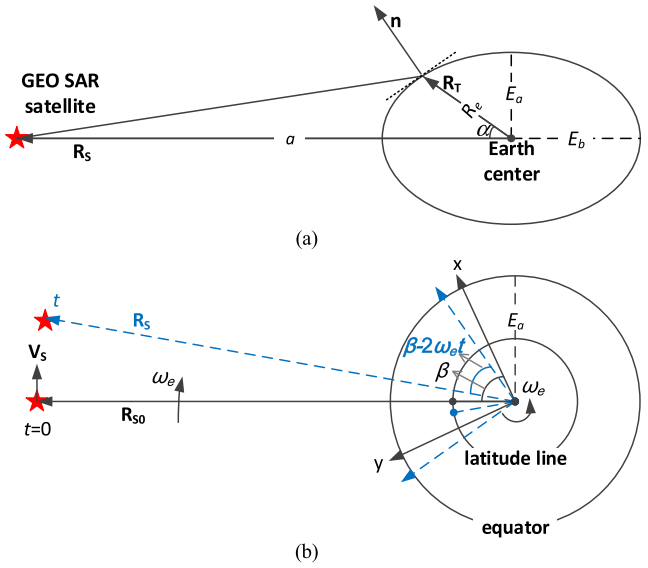

FIGURE 1. The geometric relation between the satellite and target. (a) Side looking profile of satellite, target, and Earth center. (b) Geometry from due north sight.

the equator, and the relative motion of the satellite and the Earth remains unchanged; (3) The imaging performance for targets at the same latitude is consistent, as long as the satellite system is invariable and only delayed in time.

The semi-major axis of satellite orbit is a, the rotational angular velocity of Earth is ω_e, the latitude and longitude of the given target are α and β, the distance from target to Earth center is R_e. The azimuth time is t, which is defined as $t = 0$ at the side looking time. In ECEF coordinate, $\mathbf{R_T}$ is target position vector, $\mathbf{n}$ is normal vector of target ground plane, $\mathbf{R_{S0}}$ is satellite position vector at $t = 0$. At a given time t, $\mathbf{R_S}$ and $\mathbf{V_S}$ are satellite position and velocity vectors.

In order to design a 24-hour continuous observation GEO SAR system, the imaging time of a single satellite should be determined first. For GEO SAR to achieve 2-D imaging, it is not only related to beam accessibility, but also has more requirements for observation geometry and radar parameters. In this paper, four imaging conditions about incident angle, ground resolution included angle, synthetic aperture time, and signal bandwidth are considered to determine the imaging time.

In the ground plane, the target range gradient at time t is

$$\nabla \mathbf{R} = -\frac{(\mathbf{R_S} - \mathbf{R_T}) - [(\mathbf{R_S} - \mathbf{R_T}) \bullet \mathbf{n}]\,\mathbf{n}}{|\mathbf{R_S} - \mathbf{R_T}|} \tag{1}$$

where the symbol $\bullet$ stands for the inner product operator, the target Doppler gradient at time t is

$$\nabla f_a = -\frac{\left[\mathbf{V_S} - \left(\mathbf{V_S} \bullet \frac{\mathbf{R_S}-\mathbf{R_T}}{|\mathbf{R_S}-\mathbf{R_T}|}\right)\frac{\mathbf{R_S}-\mathbf{R_T}}{|\mathbf{R_S}-\mathbf{R_T}|}\right]}{|\mathbf{R_S} - \mathbf{R_T}|} + \frac{\left\{\left[\mathbf{V_S} - \left(\mathbf{V_S} \bullet \frac{\mathbf{R_S}-\mathbf{R_T}}{|\mathbf{R_S}-\mathbf{R_T}|}\right)\frac{\mathbf{R_S}-\mathbf{R_T}}{|\mathbf{R_S}-\mathbf{R_T}|}\right] \bullet \mathbf{n}\right\}\mathbf{n}}{|\mathbf{R_S} - \mathbf{R_T}|} \tag{2}$$

As given in [19], the vectors, $\mathbf{R_S}$, $\mathbf{R_T}$, and $\mathbf{n}$, have analytical expressions, so it is more concise to calculate $\nabla \mathbf{R}$ and $\nabla \boldsymbol{f_a}$.

For each target area, at $t = 0$, the incident angle θ_{IA0} is calculated by (3). If $\theta_{\mathrm{IA0}} <$ IAMin (Acceptable minimum value of incident angle) or $\theta_{\mathrm{IA0}} >$ IAMax (Acceptable maximum value of incident angle), the target cannot be observed by this GEO SAR ConII. Otherwise, the imaging conditions are analyzed in 12 hours centered on $t = 0$.

$$\theta_{\mathrm{IA0}} = \langle \mathbf{n}, \mathbf{R_{S0}} - \mathbf{R_T} \rangle \tag{3}$$

The incident angle $\theta_{\mathrm{IA}}(t)$ is given by (4). At $t = 0$, θ_{IA0} is minimum. As t increases or decreases, $\theta_{\mathrm{IA}}(t)$ gets larger to 90° when the line of sight is tangent to Earth's surface.

$$\theta_{\mathrm{IA}}(t) = \langle \mathbf{n}, \mathbf{R_S} - \mathbf{R_T} \rangle \tag{4}$$

The ground resolution included angle between range and Doppler gradient directions θ_{GRIA} (t) is given by (5). At $t = 0$, when the side looking geometry is formed, θ_{GRIA} (t) = 90°. As t increases or decreases, θ_{GRIA} (t) gets smaller first and then gets larger to 90° again at the time when θ_{IA} (t) = 90°.

$$\theta_{\mathrm{GRIA}}(t) = \cos^{-1}\frac{\left|\nabla \mathbf{R} \bullet \nabla \boldsymbol{f}_a\right|}{|\nabla \mathbf{R}|\left|\nabla \boldsymbol{f}_a\right|} \tag{5}$$

For azimuth resolution ρ_{az}, the required synthetic aperture time $T_a(t)$ is given by (6), where λ is the wavelength. At $t = 0$, $T_a(t)$ is minimum. As t increases or decreases, $T_a(t)$ gets larger.

$$T_a(t) = \frac{\lambda}{2\rho_{az}\left|\nabla \boldsymbol{f_a}\right| \sin\theta_{\mathrm{GRIA}}(t)} \tag{6}$$

For range resolution ρ_{rg}, the required signal bandwidth $B_r(t)$ is given by (7), where c is the speed of light in vacuum. At $t = 0$, $B_r(t)$ is maximum. As t increases or decreases, $B_r(t)$ gets smaller.

$$B_r(t) = \frac{c}{2\rho_{rg}|\nabla \mathbf{R}| \sin\theta_{\mathrm{GRIA}}(t)} \tag{7}$$

According to Equations (4) to (7), we can find four time span L1, L2, L3, and L4 from four imaging conditions. First, L1 is found when $\theta_{\mathrm{IA}}(t) >$ IAMin and $\theta_{\mathrm{IA}}(t) <$ IAMax. Second, L2 is found when $\theta_{\mathrm{GRIA}}(t) >$ GRIAMin(Acceptable minimum value of ground resolution included angle). Third, L3 is found when $T_a(t) <$ SATMax (Acceptable maximum value of synthetic aperture time). Fourth, L4 is found when $B_r(t) <$ SBMax(Acceptable maximum value of signal bandwidth). Due to the geometry symmetry, L1, L2, L3, and L4 are centered on $t = 0$, the intersection of which gives the imaging time of signal GEO SAR, $\mathrm{T_{Single}}$.

B. DISTRIBUTION AND OPERATION OF GEO SAR CONSTELLATION

In case several duplicated GEO SAR satellites are launched in the same orbit, the given target can be observed continuously by constellation relay. That is, the former satellite comes into

the imaging time span first, and then the latter one comes into the imaging time span when the former one cannot satisfy imaging conditions. We assume that the satellites have 1-D roll steering capability and the antennas have 1-D azimuth scanning capability. In order to achieve 24-hour continuous observation, the way to control the rolling angle and the azimuth scanning angle under the guidance of target is established.

To fulfill continuous observation, the numbers of GEO SAR satellites that composes the constellation is given by $N_{Constellation} = \lceil 12/T_{Single} \rceil$, where $\lceil \cdot \rceil$ calculates the nearest integer toward infinity. Then, the imaging time of each GEO SAR in constellation is renewed as follows:

$$T_{Constellation} = \frac{12}{N_{Constellation}} \tag{8}$$

In an optimized design, the satellite would be evenly distributed in longitude, and the longitude difference can be expressed as

$$LON_{Dif} = \frac{360}{N_{Constellation}} \tag{9}$$

To move the beam center line to the given target, the rolling angle is set by (10). If the target locates in northern hemisphere, the satellite platform turns right where the rolling angle is defined as positive, and vice versa. At $t = 0$, $\theta_{roll}(t)$ is maximum. As t increases or decreases, $\theta_{roll}(t)$ gets smaller.

$$\theta_{roll}(t) = \tan^{-1} \frac{R_e \sin\alpha}{a - R_e \cos\alpha \cos(2\omega_e t)} \tag{10}$$

To move the beam center point to the given target, the azimuth angle is set by (11). At $t = 0$, $\theta_{sq}(t) = 0°$. As t increases, $\theta_{sq}(t)$ gets larger to minus direction. As t decreases, $\theta_{sq}(t)$ gets larger to plus direction.

$$\theta_{sq}(t) = -\sin^{-1} \frac{R_e \cos\alpha \sin(2\omega_e t)}{|\mathbf{R}_S - \mathbf{R}_T|} \tag{11}$$

The given GEO SAR constellation running on the equatorial geosynchronous orbit share the same orbit with those geostationary commercial communication satellites, [20] and [21]. The collision cannot be occurred between the satellites in constellation. The collision between the constellation and the other commercial communication satellites can be avoided by increasing or decreasing the orbit height to some extent. By the way, this change has no effect on the overall design of the constellation and the subsequent analysis of the signal characteristics.

C. SIMULATION

In the following, an example of GEO SAR ConII is demonstrated. The range and azimuth resolution in ground plane is set to be 5m. The L-band (wavelength 24cm) is chosen, as that in [13]. The imaging conditions are shown in Table 1.

The area required for 24-hour continuous observing is from 20°N to 45°N. Two representative cities (Harbin and Haikou) are selected at the latitude edges, the locations of which are shown in Table 2.

TABLE 1. Imaging conditions.

SATMax	SBMax	IAMin	IAMax	GRIAMin
300s	100MHz	10°	70°	30°

TABLE 2. Location of two representative cities.

City	Harbin	Haikou
Central longitude	126.68°E	110.33° E
Central latitude	45.75°N	20.03°N

TABLE 3. Constellation parameters.

Parameters	Value
$T_{Constellation}$	2.4 h
$N_{Constellation}$	5
LON_{Dif}	72°
Maximum rolling angle	6.88°
Maximum azimuth angle	5.37°

According to Equations (4) to (7), the available imaging time of Harbin is 3.134h (1.567h before its side looking time and 1.567h after) and that of Haikou is 2.666h (1.333h before its side looking time and 1.333h after).Therefore, five satellites are required for 24-hour continuous observation. According to Equation (10), the rolling angle required for Harbin is more demanding which is from 6.73deg to 6.88deg. According to Equation (11), the azimuth angle required for Haikou is more demanding, which is from -5.37deg to 5.37deg.The parameters of the constellation are shown in Table 3.

The observation capability of GEO SAR ConII based on the parameters in Table 3 is compared with that of ConI by simulations. The radar parameters and imaging conditions are coherent except that, in ConI, the SATMax is added four times to 1200s and the satellite number is doubled.

The global imaging time of the two constellations are compared in Fig. 2. The simulation results show that the ConI has global imaging capability, whereas the ConII cannot image the low-latitude and high-latitude areas.

The average imaging time across all longitudes with respect to latitude of ConI and ConII are compared in Fig. 3. It can be seen that, in the latitude range from 15 degrees to 50 degrees in both south and north hemisphere, the ConII can realize 24-hour imaging, which is superior to ConI.

The imaging time varying with longitude of ConI and ConII are compared in Fig. 4, for latitudes of Harbin and Haikou. The simulation results show that, for certain latitude, the imaging time of ConII remains unchanged with longitude, but that of ConI fluctuates greatly.

The average synthetic aperture time across all longitudes with respect to latitude of ConI and ConII are compared in Fig. 5. The synthetic aperture time of Harbin and Haikou in one orbital period (24h) are shown in Fig. 6. The simulation results show that: (1) In the mid-latitude area, the average synthetic aperture time of ConII is between 180s and 200s, and that of ConI is between 450s and 550s. (2) The synthetic aperture time in ConII of Harbin is from 150s to 180s, and

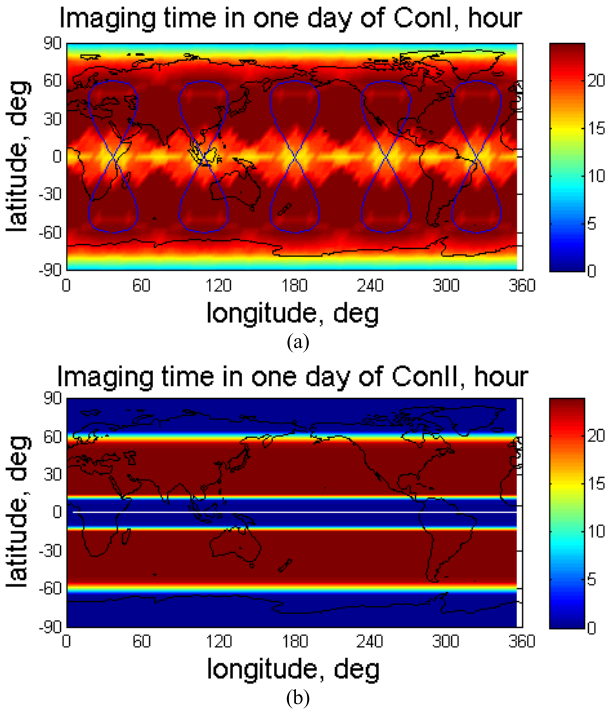

FIGURE 2. Global imaging time. (a) ConI.(b) ConII.

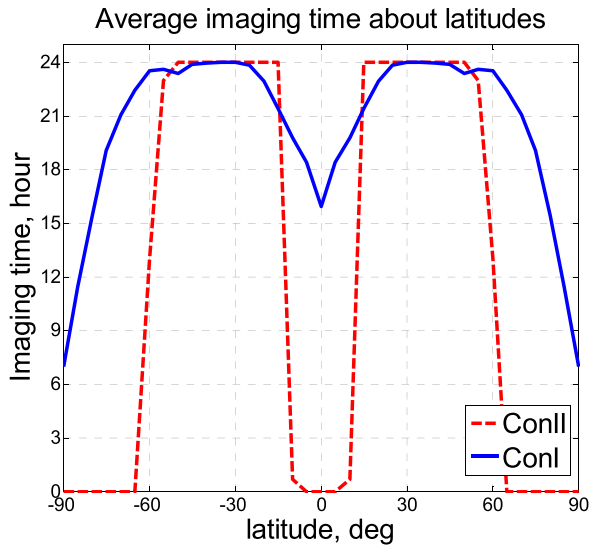

FIGURE 3. Average imaging time across all longitudes with respect to latitude of ConI and ConII.

that of Haikou is from 140s to 280s, meanwhile that in ConI of Harbin is from 300s to 1300s, and that of Haikou is from 350s to 700s. Compared with ConI, the synthetic aperture time of ConII is shortened more than a half, and changes with regularity, which is a notable feature.

III. ACCURATE SLANT RANGE MODELING

A. LINEAR APPROXIMATION OF RANGE HISTORY WITHIN ONE PULSE PROCESS

GEO SAR has a very high orbital altitude, the imaging distance of which exceeds 36,000 km. During the time from

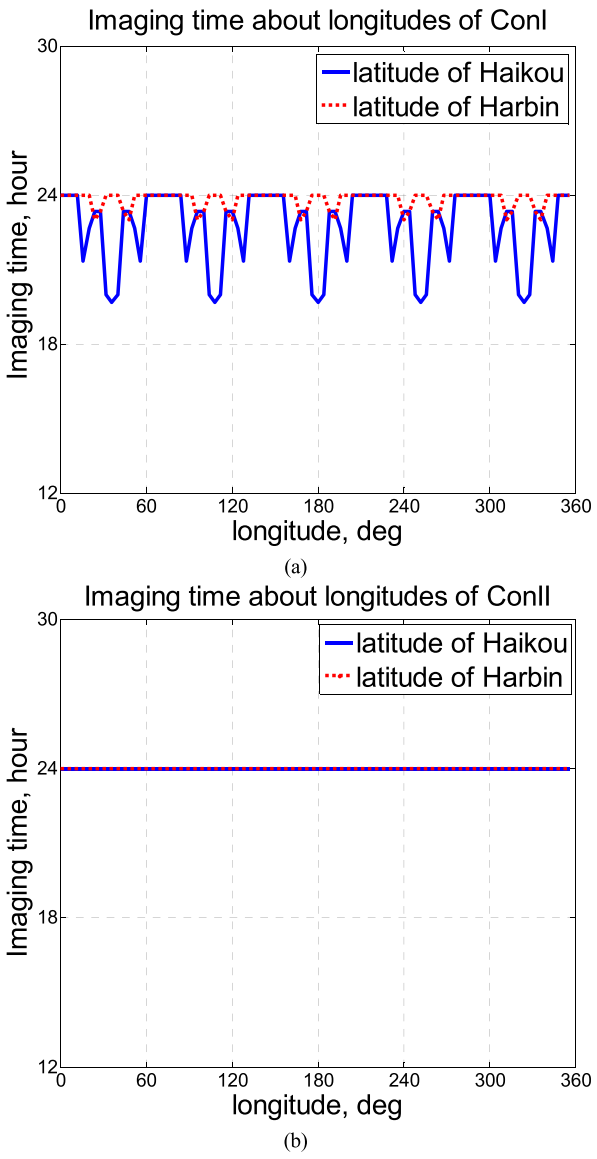

FIGURE 4. Imaging time varying with longitude of two specific latitudes. (a) ConI. (b) ConII.

transmitting to receiving one pulse signal, the relative motion between satellite and ground causes that the transmitting slant range and the receiving slant range are no longer equal. Moreover, since the given GEO SAR system adopts the squint technology to observe continuously and the large pulse width signal to enhance transmission power (The pulse width is set to be 1ms in [13], [22]), the signal distortion caused by relative motion during pulse transmission period and reception period is not negligible. Therefore, the stop-and-go assumption is no longer valid.

The comparison of the three relative motion models is shown in Fig. 7. As shown in left figure, the range history is kept constant during the period from transmission to reception of one pulse (of hundreds of ms level), which is based on the traditional stop-and-go assumption. As shown in middle figure, the transmitting range history is kept constant during

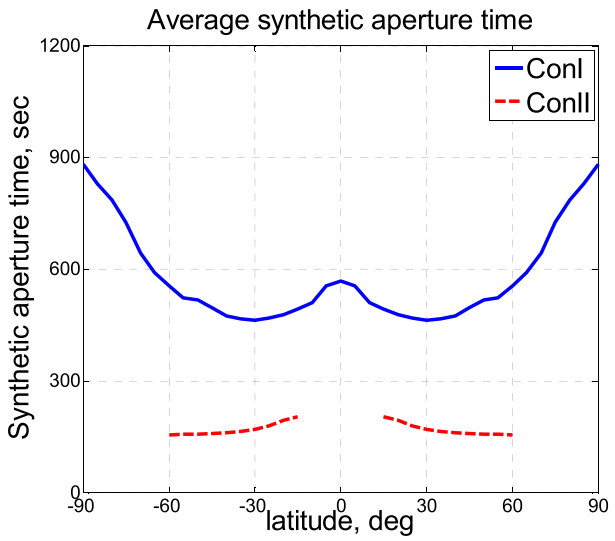

FIGURE 5. Average synthetic aperture time across all longitudes with respect to latitude of ConI and ConII.

the transmission period and the receiving range history is kept constant during the reception period (of hundreds of μs level), which is based on the inner pulse stop-and-go assumption. As shown in right figure, the range history is changing all the time, which is the foundation of this paper.

In order to describe the effect of continuous satellite and ground motion on range history, this paper establishes the variation of slant range with both the slow and the fast time. The fast time axis is set as τ, and slow time axis is set as η. When the signal is received at time $\eta + \tau$, it has experienced the transmitting slant range $R_{\mathrm{Tr}}(\eta + \tau)$ from SAR antenna to target and the receiving slant range $R_{\mathrm{Re}}(\eta + \tau)$ from target to SAR antenna. Since the reception duration is very short, it can be considered that $R_{\mathrm{Tr}}(\eta + \tau)$ and $R_{\mathrm{Re}}(\eta + \tau)$ change linearly with fast time τ in terms of slope $V_{\mathrm{Tr}}(\eta)$ and $V_{\mathrm{Re}}(\eta)$, respectively. The linear approximations are given as follows:

$$R_{\mathrm{Tr}}(\eta + \tau) = R_{\mathrm{Tr}}(\eta) + V_{\mathrm{Tr}}(\eta)\,\tau \tag{12}$$

$$R_{\mathrm{Re}}(\eta + \tau) = R_{\mathrm{Re}}(\eta) + V_{\mathrm{Re}}(\eta)\,\tau \tag{13}$$

If the transmitting and receiving range can be accurately calculated, their changing slope can be obtained by taking derivatives.

B. RANGE CALCULATION BASED ON CURVILINEAR MOTION OF CONSTANT ACCELERATION

In order to accurately calculate the two-way slant range, it is generally necessary to obtain the propagation delay from transmitting to receiving the pulse by iterative method. However, the iterative method will greatly increase the calculation amount and time. In [22], the uniformly linear motion of satellite and Earth is used to get the analytical solution for propagation delay calculation.

In view of the satellite orbital motion and the Earth's rotation, the uniform acceleration curve motion is used instead in the following. During the period from transmitting to receiving one pulse, it is assumed that the acceleration of satellite and target remains constant and the velocity keeps uniformly changing, which is illustrated in Fig. 8.

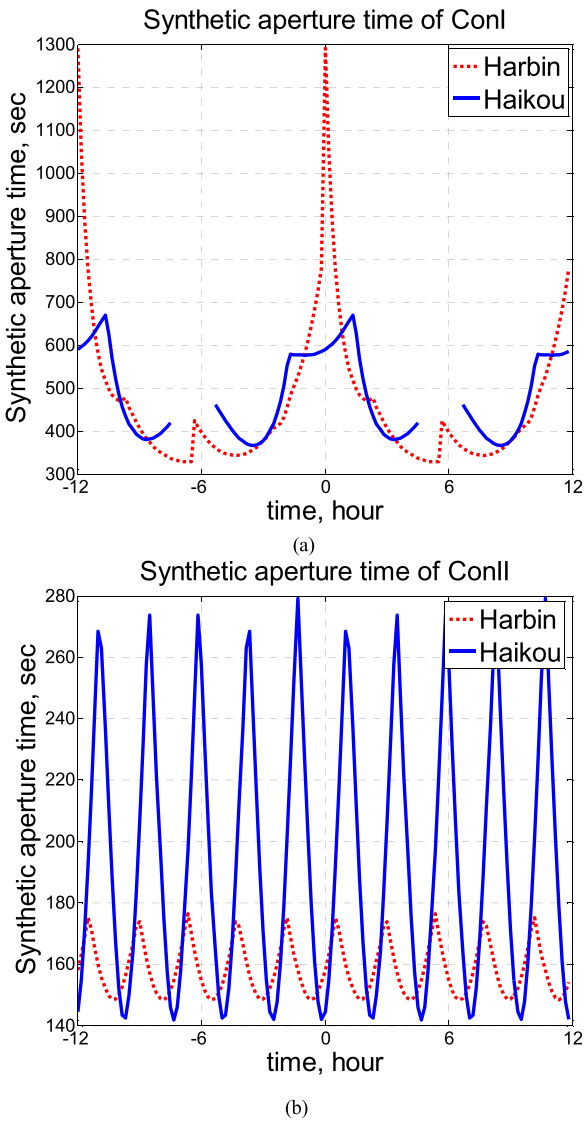

FIGURE 6. Synthetic aperture time of Harbin and Haikou in 24h. (a) ConI.(b) ConII.

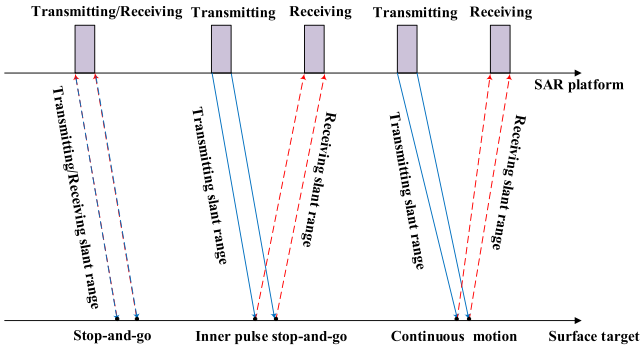

FIGURE 7. Comparison between the stop-and-go assumption, the inner pulse stop-and-go assumption, and the continuous satellite and ground motion.

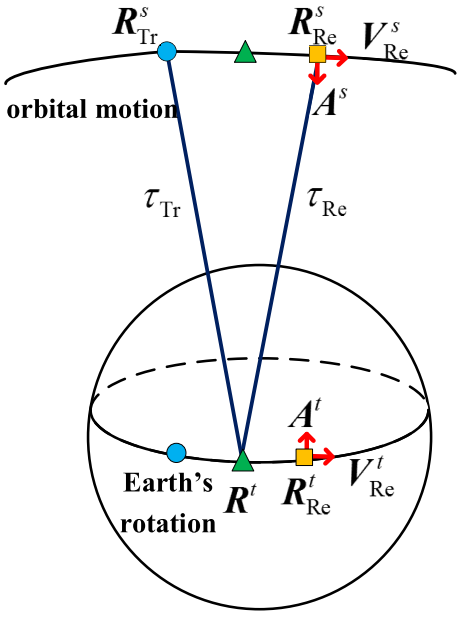

FIGURE 8. The uniform acceleration curve motion of the satellite and the target.

In Fig. 8, at the transmitting moment (marked by circle), the satellite position vector is denoted by $\boldsymbol{R}^s_{\mathrm{Tr}}$. After transmission delay τ_{Tr} (marked by triangle), the target position vector is denoted by $\boldsymbol{R}^t$. After reception delay τ_{Re} (marked by square), the position and velocity vectors of satellite are denoted by $\boldsymbol{R}^s_{\mathrm{Re}}$ and $\boldsymbol{V}^s_{\mathrm{Re}}$, and those of target are denoted by $\boldsymbol{R}^t_{\mathrm{Re}}$ and $\boldsymbol{V}^t_{\mathrm{Re}}$.The acceleration vector of satellite and target are constant within one pulse period, which are demoted by $\boldsymbol{A}^s$ and $\boldsymbol{A}^t$.

According to the uniform acceleration curve motion of target, we have $\boldsymbol{R}^t = \boldsymbol{R}^t_{\mathrm{Re}} - \boldsymbol{V}^t_{\mathrm{Re}}\tau_{\mathrm{Re}} - \frac{1}{2}\boldsymbol{A}^t\tau^2_{\mathrm{Re}}$. The receiving delay τ_{Re} meets the equation as follows:

$$\left\|\boldsymbol{R}^t - \boldsymbol{R}^s_{\mathrm{Re}}\right\| = c\tau_{\mathrm{Re}} \tag{14}$$

Rearranging the equation (14), we can get the quartic equation of τ_{Re} as follows:

$$a_4\tau^4_{\mathrm{Re}} + a_3\tau^3_{\mathrm{Re}} + a_2\tau^2_{\mathrm{Re}} + a_1\tau_{\mathrm{Re}} + a_0 = 0 \tag{15}$$

In equation (15), the coefficients of the quartic equation are given by:

$$\begin{aligned}
a_4 &= \frac{1}{4}\left\|\boldsymbol{A}^t\right\|^2 \\
a_3 &= \left\langle \boldsymbol{V}^t_{\mathrm{Re}}, \boldsymbol{A}^t \right\rangle \\
a_2 &= \left\|\boldsymbol{V}^t_{\mathrm{Re}}\right\|^2 + \left\langle \boldsymbol{R}^s_{\mathrm{Re}} - \boldsymbol{R}^t_{\mathrm{Re}}, \boldsymbol{A}^t \right\rangle - c^2 \\
a_1 &= 2\left\langle \boldsymbol{R}^s_{\mathrm{Re}} - \boldsymbol{R}^t_{\mathrm{Re}}, \boldsymbol{V}^t_{\mathrm{Re}} \right\rangle \\
a_0 &= \left\|\boldsymbol{R}^s_{\mathrm{Re}} - \boldsymbol{R}^t_{\mathrm{Re}}\right\|^2
\end{aligned} \tag{16}$$

Solving this quartic equation, four solutions are obtained, including two negative numbers and two positive numbers. The smaller positive number is the effective result for τ_{Re}.

Similarly, according to the uniform acceleration curve motion of satellite, we have $\boldsymbol{R}^s_{\mathrm{Tr}} = \boldsymbol{R}^s_{Re} - \boldsymbol{V}^s_{\mathrm{Re}}(\tau_{\mathrm{Re}} + \tau_{\mathrm{Tr}}) - \frac{1}{2}\boldsymbol{A}^s(\tau_{\mathrm{Re}} + \tau_{\mathrm{Tr}})^2$.

The transmitting delay τ_{Tr} satisfies:

$$\left\|\boldsymbol{R}^s_{\mathrm{Tr}} - \boldsymbol{R}^t\right\| = c\tau_{Tr} \tag{17}$$

Rearranging the equation (17), we can get the quartic equation of τ_{Tr} as follows:

$$b_4\tau^4_{\mathrm{Tr}} + b_3\tau^3_{\mathrm{Tr}} + b_2\tau^2_{\mathrm{Tr}} + b_1\tau_{\mathrm{Tr}} + b_0 = 0 \tag{18}$$

In equation (18), the coefficients of the quartic equation are given by:

$$\begin{aligned}
b_4 &= \frac{1}{4}\left\|\boldsymbol{A}^s\right\|^2 \\
b_3 &= \left\langle \boldsymbol{V}^s_{\mathrm{Re}} + \boldsymbol{A}^s\tau_{\mathrm{Re}}, \boldsymbol{A}^s \right\rangle \\
b_2 &= \left\|\boldsymbol{V}^s_{\mathrm{Re}} + \boldsymbol{A}^s\tau_{\mathrm{Re}}\right\|^2 \\
&\quad - \left\langle \boldsymbol{R}^s_{\mathrm{Re}} - \boldsymbol{R}^t_{\mathrm{Re}} - \left(\boldsymbol{V}^s_{\mathrm{Re}} - \boldsymbol{V}^t_{\mathrm{Re}}\right)\tau_{\mathrm{Re}} \right. \\
&\quad \left. - \frac{1}{2}\left(\boldsymbol{A}^s - \boldsymbol{A}^t\right)\tau^2_{\mathrm{Re}}, \boldsymbol{A}^s \right\rangle - c^2 \\
b_1 &= -2\left\langle \boldsymbol{R}^s_{\mathrm{Re}} - \boldsymbol{R}^t_{\mathrm{Re}} - \left(\boldsymbol{V}^s_{\mathrm{Re}} - \boldsymbol{V}^t_{\mathrm{Re}}\right)\tau_{\mathrm{Re}} \right. \\
&\quad \left. - \frac{1}{2}\left(\boldsymbol{A}^s - \boldsymbol{A}^t\right)\tau^2_{\mathrm{Re}}, \boldsymbol{V}^s_{\mathrm{Re}} + \boldsymbol{A}^s\tau_{\mathrm{Re}} \right\rangle \\
b_0 &= \left\| \boldsymbol{R}^s_{\mathrm{Re}} - \boldsymbol{R}^t_{\mathrm{Re}} - \left(\boldsymbol{V}^s_{\mathrm{Re}} - \boldsymbol{V}^t_{\mathrm{Re}}\right)\tau_{\mathrm{Re}} - \frac{1}{2}\left(\boldsymbol{A}^s - \boldsymbol{A}^t\right)\tau^2_{\mathrm{Re}} \right\|^2
\end{aligned} \tag{19}$$

Solving this equation, the smaller positive number is the solution for τ_{Tr}.

Through the above steps, the two-way slant range $R_{\mathrm{Tr}}(\eta) + R_{\mathrm{Re}}(\eta)$ at any given time can be acquired, and the variation slope $V_{\mathrm{Tr}}(\eta) + V_{\mathrm{Re}}(\eta)$ can be obtained by taking derivatives.

C. SIMULATION

The simulation results given below reveal the range model error caused by the four motion assumptions, including the stop-and-go assumption, the uniform velocity linear motion, the uniform acceleration curve motion, and the MHRE model. The parameters of satellite and SAR systems follow those in Section II. The iterative method is used to calculate the accurate two-way slant range.

Fig. 9 shows the range model error of the point target located in Haikou at side looking and squint looking geometry, where the squint angles are 0deg and 5.37deg respectively. The error caused by stop-and-go assumption is composed of constant term and linear term. The constant term becomes negligible in side looking geometry and reaches 70m in squint looking geometry. The linear term maintains at about 10m in two geometries. The error caused by uniform velocity linear motion is also composed of constant term and linear term. The constant term reaches 0.0139m in squint looking geometry, which will cause constant phase error of 41.7° and further cause deviation to some applications like interferometry. The Doppler center frequency deviation caused by the linear term error is less than 1Hz, which can be ignored. What's more, the error based on uniform velocity linear motion is 10^{-2}m

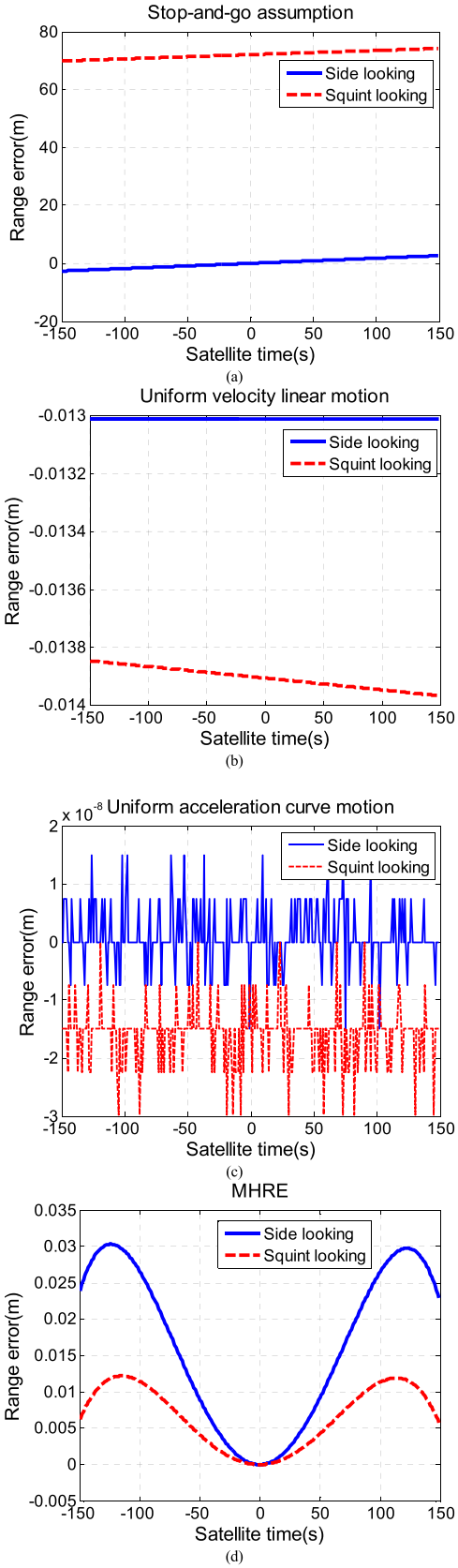

FIGURE 9. Different range model error. (a) Based on stop-and-go assumption. (b) Based on uniform velocity linear motion. (c) Based on uniform acceleration curve motion. (d) Base on MHRE.

orders of magnitude, whereas the error based on uniform acceleration curve motion is only 10^{-8}m orders of magnitude. It means that, the range model precision is enhanced by 6 orders of magnitude. According to the trend of the range error, the error based on uniform velocity linear motion increases linearly as the synthetic aperture time extends. Meanwhile, the error based on uniform acceleration curve motion is kept at 10^{-8}m orders of magnitude. The error based on MRHE includes quadratic and quartic terms, the maximum value is 0.03m, which will cause phase error of 90°. The precision of MRHE is not appropriate for the proposed GEO SAR. Therefore, we can get better precision by the proposed range model, which can be applied to conditions with higher requirements of precision. Similarly, through the simulation results of Harbin, we can come to the same conclusion.

IV. SIGNAL MODEL AND CHARACTERISTICS

A. SIGNAL MODEL IN 2-D TIME DOMAIN

The signal model of GEO SAR is established according to the accurate slant range given above. The quadrature demodulated baseband signal is written by:

$$\begin{aligned} s(\tau,\eta) = {} & \mathrm{rect}\left\{\frac{1}{T}\left[\tau-\frac{2}{c}R(\eta+\tau)\right]\right\} \\ & \times \exp\left\{j\pi k_r\left[\tau-\frac{2}{c}R(\eta+\tau)\right]^2\right\} \\ & \times w_a(\eta)\exp\left\{-j\frac{4\pi f_c}{c}R(\eta+\tau)\right\} \end{aligned} \tag{20}$$

where, rect () is the unit rectangular window, k_r and T are the chirp rate and pulse width of the transmitted chirp pulse, w_a () is the antenna beam pattern in azimuth direction, f_c is the radar carrier frequency, R () is the average of one-way range history.

In terms of the linear approximation given in equation (12) and (13), we have:

$$R(\eta+\tau) = R(\eta) + V(\eta)\tau \tag{21}$$

where $R(\eta) = \frac{1}{2}R_{\mathrm{Tr}}(\eta) + \frac{1}{2}R_{\mathrm{Re}}(\eta)$, $V(\eta) = \frac{1}{2}V_{\mathrm{Tr}}(\eta) + \frac{1}{2}V_{\mathrm{Re}}(\eta)$.

By substituting equation (21) into equation (20), we can get

$$\begin{aligned} s(\tau,\eta) = {} & \mathrm{rect}\left\{\frac{1-\frac{2}{c}V(\eta)}{T}\left[\tau-\frac{2}{c}\left(\frac{R(\eta)}{1-\frac{2}{c}V(\eta)}\right)\right]\right\} \\ & \times \exp\left\{j\pi k_r\left(1-\frac{2}{c}V(\eta)\right)^2\right. \\ & \left.\times\left[\tau-\frac{2}{c}\left(\frac{R(\eta)}{1-\frac{2}{c}V(\eta)}\right)\right]^2\right\} w_a(\eta) \\ & \times \exp\left\{-j\frac{4\pi f_c}{c}\left(1-\frac{2}{c}V(\eta)\right)\left(\frac{R(\eta)}{1-\frac{2}{c}V(\eta)}\right)\right. \\ & \left.-\frac{j4\pi f_c V(\eta)\tau}{c}\right\} \end{aligned} \tag{22}$$

Rearranging the equation (22), we can get

$$\begin{aligned} & s(\tau, \eta) \\ & = \operatorname{rect}\left\{\frac{1}{T+\Delta T}\left[\tau-\frac{2}{c}(R(\eta)+\Delta R)\right]\right\} \\ & \quad \times \exp\left\{j\pi(k_r+\Delta k_r)\left[\tau-\frac{2}{c}(R(\eta)+\Delta R)\right]^2\right\} w_a(\eta) \\ & \quad \times \exp\left\{-j\frac{4\pi}{c}(f_c+\Delta f_c)(R(\eta)+\Delta R)+j2\pi\Delta f_c\tau\right\} \end{aligned} \tag{23}$$

where Δf_c, Δk_r, ΔT, ΔR respectively represent the amount of change in carrier frequency, chirp rate, pulse width and slant range, all of which depend on the azimuth time. It reveals the modulation effects induced by the slant range variation within one pulse process, by contrast with the traditional signal model.

Let the instantaneous Doppler frequency history is $f_d(\eta)$, where $f_d(\eta) = -2V(\eta)/\lambda$, we have:

$$\frac{\Delta f_c}{f_c} = \frac{f_d(\eta)}{f_c} \tag{24}$$

$$\frac{\Delta k_r}{k_r} = \left[1+\frac{f_d(\eta)}{f_c}\right]^2 - 1 \tag{25}$$

$$\frac{\Delta T}{T} = -\frac{f_d(\eta)}{f_c+f_d(\eta)} \tag{26}$$

$$\frac{\Delta R}{R(\eta)} = -\frac{f_d(\eta)}{f_c+f_d(\eta)} \tag{27}$$

It shows that the modulation degree has positive correlation with the Doppler frequency and negative correlation with the carrier frequency. Thus, the higher the resolution and the larger the squint angle, the more serious is the modulation effects. The lower the radar carrier frequency, the more serious is the effects.

B. SIGNAL MODEL IN 2-D FREQUENCY DOMAIN

The range Fourier transform is applied to the signal in 2-D time domain, and the expression of the signal in range frequency and azimuth time domain is obtained as follows:

$$\begin{aligned} s(f, \eta) = & \operatorname{rect}\left[\frac{f-\Delta f_c}{(k_r+\Delta k_r)(T+\Delta T)}\right] w_a(\eta) \\ & \times \exp\{j[\psi_0(f, \eta)+\psi_1(f, \eta)+\psi_2(f, \eta)]\} \end{aligned} \tag{28}$$

where, f is the range frequency axis, and the range bandwidth varies $1+[f_d(\eta)/f_c]$ times. The phase includes three terms. $\psi_0(f, \eta)$ has the same expression with that of the traditional signal model. $\psi_1(f, \eta)$ and $\psi_2(f, \eta)$ reveal the modulation in range and azimuth signal respectively, which are given by:

$$\psi_1(f, \eta) = -\pi\frac{(f-\Delta f_c)^2}{k_r+\Delta k_r} + \pi\frac{f^2}{k_r} \tag{29}$$

$$\psi_2(f, \eta) = -\frac{4\pi}{c}(f_c+f)\Delta R \tag{30}$$

Performing azimuth Fourier transform on the signal in range frequency and azimuth time domain. Since the magnitude of $\psi_1(f, \eta)$ and $\psi_2(f, \eta)$ is much less than that of $\psi_0(f, \eta)$, by ignoring the effect of these two terms on the solution of stationary phase expression, we can get

$$\xi = \left(1+\frac{f}{f_c}\right) f_d(\eta) \tag{31}$$

where ξ is the azimuth frequency axis. By substituting equation (31) into equation (28), the signal in 2-D frequency domain can be expressed as:

$$\begin{aligned} s(f, \xi) = & \operatorname{rect}\left\{\frac{f-\xi/(f/f_c+1)}{k_r T[1+\xi/(f+f_c)]}\right\} w_a[\eta(\xi)] \\ & \times \exp\{j[\psi_0(f, \xi)+\psi_1(f, \xi)+\psi_2(f, \xi)]\} \end{aligned} \tag{32}$$

The phase expression in 2-D frequency domain includes three terms, where $\psi_0(f, \xi)$ also has the same expression with that of the traditional signal model, $\psi_1(f, \xi)$ and $\psi_2(f, \xi)$ are given by:

$$\psi_1(f, \xi) = -\pi\frac{[f-\xi/(f/f_c+1)]^2}{k_r[1+\xi/(f+f_c)]^2} + \frac{\pi f^2}{k_r} \tag{33}$$

$$\psi_2(f, \xi) = \frac{4\pi}{c}\left[\frac{\xi}{1+\xi/(f_c+f)}\right] R(\eta(\xi)) \tag{34}$$

It shows that $\psi_1(f, \xi)$ is independent of target position but dependent on range frequency and azimuth frequency. Therefore, batch processing in 2-D frequency domain is fit for $\psi_1(f, \xi)$ compensation. Meanwhile, $\psi_2(f, \xi)$ is dependent on range frequency, azimuth frequency, and target position, which needs block processing for compensation.

In practical applications, the spaceborne SAR parameters are generally satisfied: $f_c/(f+f_c) \approx 1, \xi/(f+f_c) \ll 1$. Therefore, Equation (33) can be approximated as: $\psi_1(f, \xi) \approx 2\pi f\xi/k_r$. It is degraded to the linear term to compensate the stop-and-go assumption in the 2D frequency domain in [15].

C. SIMULATION

In order to verify the signal model in this paper, we generate the echo of the point target, conduct matched filtering in 2-D frequency domain, and then test the imaging qualities. Two matched filter functions are compared. The first one is based on the traditional signal model by calculating the slant range according to the uniform velocity linear motion [22] and by compensating $\psi_0(f, \xi)$ and $2\pi f\xi/k_r$ [15]. The second one is based on the modified signal model given in this paper by calculating the slant range according to the uniform acceleration curve motion and by compensating $\psi_0(f, \xi)$, $\psi_1(f, \xi)$ and $\psi_2(f, \xi)$.

The point target is located in the central area of Haikou. The side looking geometry and squint looking geometry are both shown. In squint case, the edge of a single satellite observable orbit arc is used. The main simulation parameters are shown in Table 4. As the squint angle increases, the imaging parameters f_s ,B_r, and T decrease correspondingly. According to equations (6) and (7), the theoretical values of both range and azimuth resolution in ground plane are approximately 2m and 5m respectively.

Fig. 10 and Fig. 11 compare the compressed targets after matched filtering based on the traditional signal model

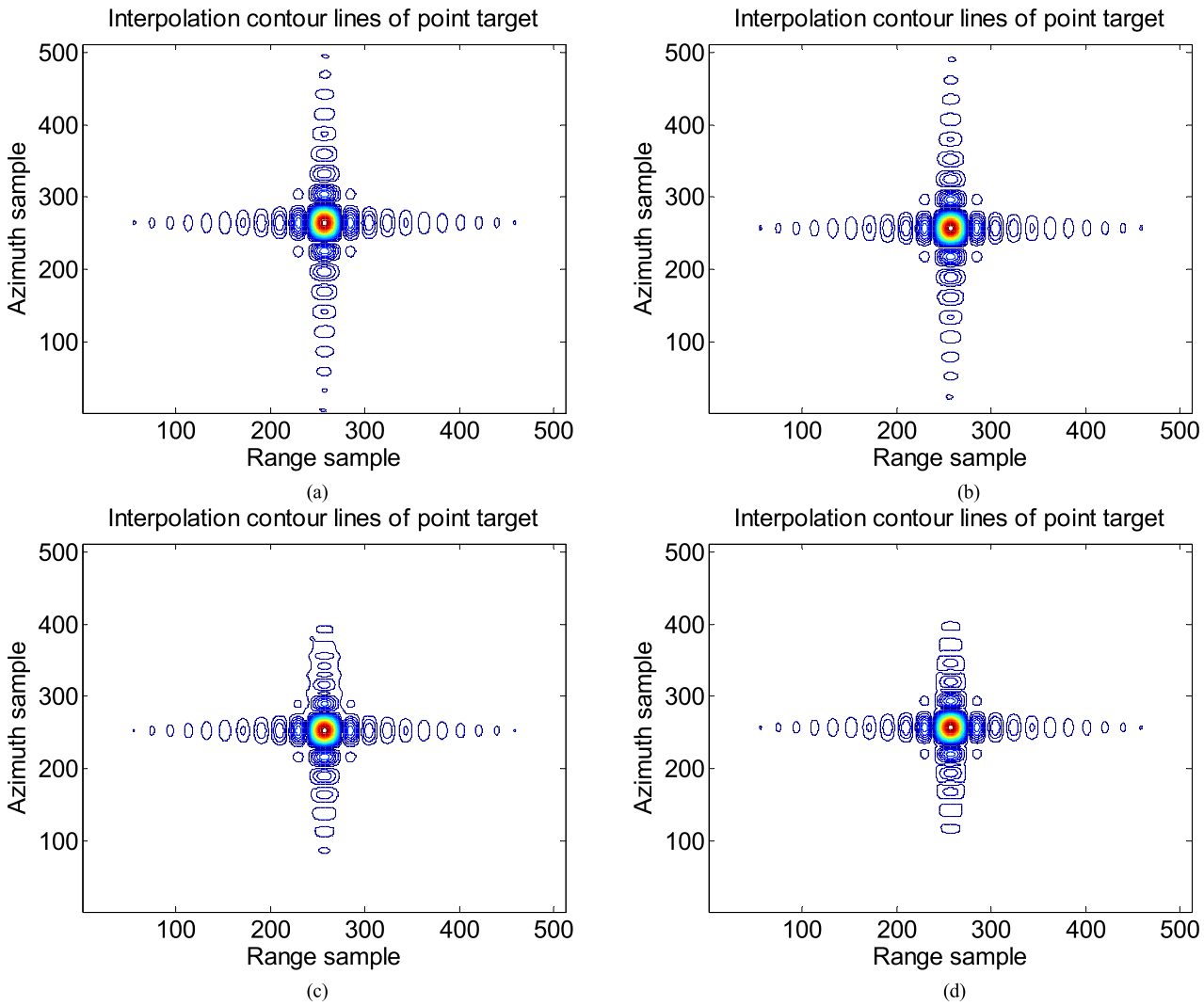

FIGURE 10. In side looking geometry, contour plots of compressed point target by 16 times interpolation. (a) 5m resolution, based on traditional signal model. (b) 5m resolution, based on modified signal model. (c) 2m resolution, based on traditional signal model. (d) 2m resolution, based on modified signal model.

TABLE 4. Simulation parameters.

Resolution		5m		2m		
Radar parameters	Symbol	Value1(Side)	Value2(Squint)	Value3(Side)	Value4(Squint)	Unit
Range sampling rate	f_s	89.8	72.8	224.6	182.0	MHz
Chirp bandwidth	B_r	74.9	60.7	187.1	151.7	MHz
Chirp duration	T	116.9	94.7	292.2	236.8	μs
Carrier frequency	f_c	1.25	1.25	1.25	1.25	GHz
Synthetic aperture time	T_a	142	277	354	694	s
Pulse repetition frequency	PRF	300	800	700	1500	Hz
Ground resolution included angle	θ_{GRIA}	90	42.6	90	42.6	deg

and modified signal model. In the side looking geometry, as shown in Fig. 10, at 5m resolution, the focused quality of both models is high; at 2m resolution, the focused quality in azimuth direction based on traditional signal model deteriorates a little. In the squint looking geometry, as shown in Fig. 11, at 5m resolution, the side lobes of azimuth direction based on traditional signal model begin to rise; at 2m resolution, the mismatch of the matched filter based on

TABLE 5. Comparison of imaging qualities at resolution of 5m.

Geometry	Model	Direction	Broadening	Resolution (m)	PSLR(dB)	ISLR(dB)
Side looking	Traditional	Range	1.06	1.877	-13.286	-10.029
		Azimuth	0.98	4.690	-13.268	-10.298
	Modified	Range	1.06	1.877	-13.282	-10.023
		Azimuth	0.99	4.690	-13.314	-10.310
Squint looking	Traditional	Range	1.00	2.188	-13.281	-10.046
		Azimuth	1.01	3.384	-11.972	-9.378
	Modified	Range	1.06	2.316	-13.279	-10.026
		Azimuth	1.00	3.342	-13.277	-10.746

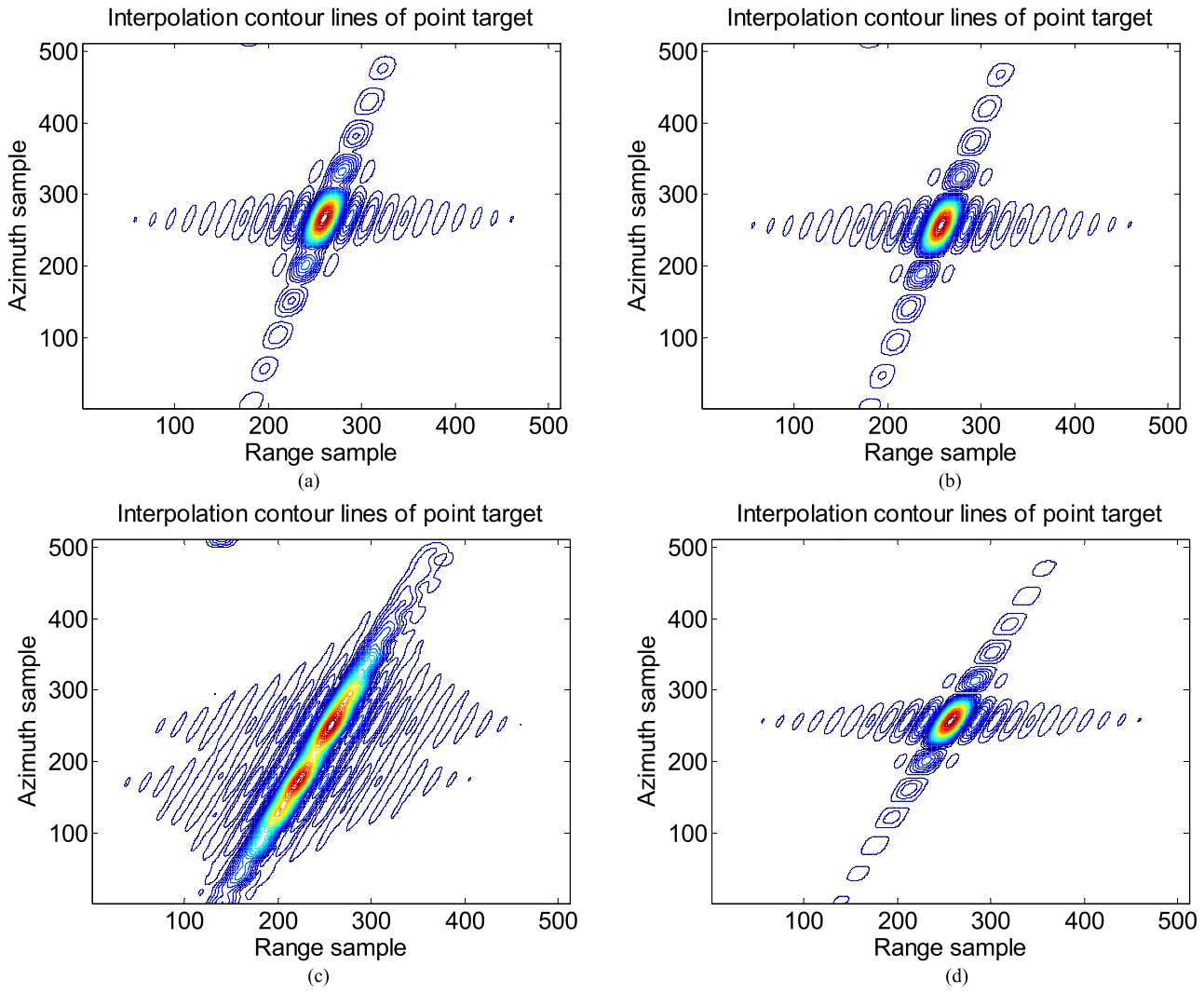

FIGURE 11. In squint looking geometry, contour plots of compressed point target by 16 times interpolation. (a) 5m resolution, based on traditional signal model. (b) 5m resolution, based on modified signal model. (c) 2m resolution, based on traditional signal model. (d) 2m resolution, based on modified signal model.

traditional signal model is significant, and the point target is totally defocused. Meanwhile, the matched filter constructed based on modified signal model can focus the target very well. The improvement in focusing quality is brought by modified signal model. The larger the squint angle is, the more obvious the improvement is.

The imaging qualities in range and azimuth directions at resolution of 5m and 2m are shown in the Table 5 and 6

TABLE 6. Comparison of imaging qualities at resolution of 2m.

Geometry	Model	Direction	Broadening	Resolution (m)	PSLR(dB)	ISLR(dB)
Side looking	Traditional	Range	1.06	0.751	-13.303	-10.039
		Azimuth	0.99	1.884	-13.176	-10.642
	Modified	Range	1.06	0.751	-13.279	-10.013
		Azimuth	0.99	1.882	-13.400	-10.615
Squint looking	Traditional	Range	1.00	0.875	-13.297	-10.077
		Azimuth	2.04	2.726	-0.019	16.784
	Modified	Range	1.06	0.927	-13.278	-10.018
		Azimuth	0.99	1.332	-13.363	-10.715

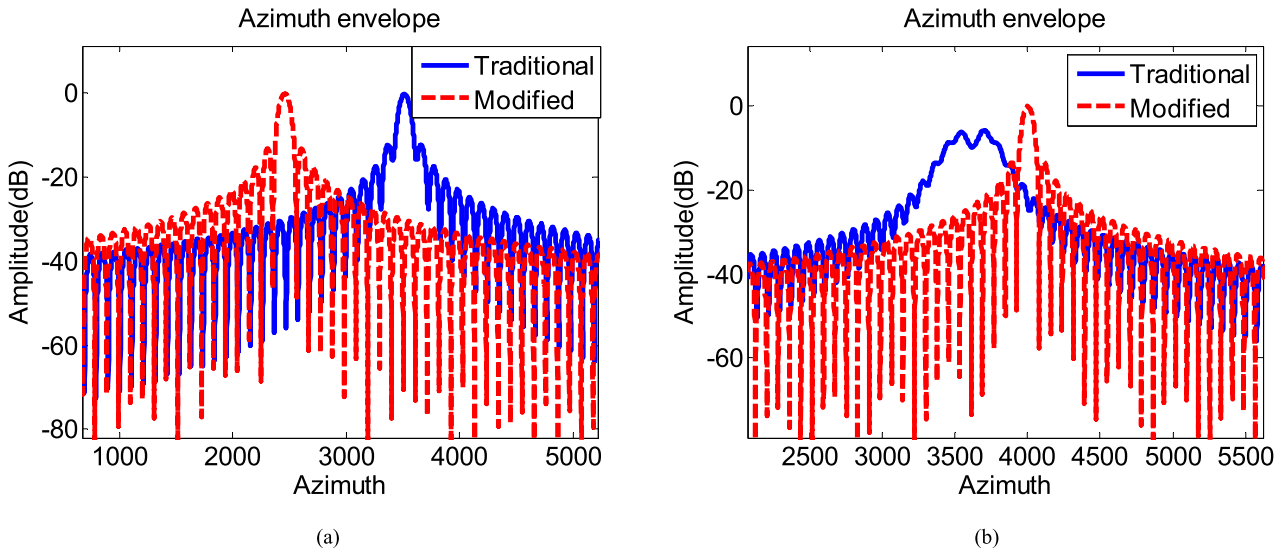

FIGURE 12. Azimuth profiles of traditional and modified signal models in squint looking geometry. (a) 5m resolution. (b) 2m resolution.

respectively. In squint looking geometry at 5m resolution, the azimuth PSLR and ISLR have deteriorated slightly based on the traditional signal model, as given in Fig. 12(a); at 2m resolution, the azimuth broadening, PSLR, and ISLR reach 2.04, −0.02dB, and 16.78dB by traditional signal model, that is the consequence of azimuth envelope of two main lobes, as given in Fig. 12(b). Those imaging qualities improve to 0.99, −13.36dB, and −10.72dB by modified signal model, which are close to the ideal values in terms of the rectangular window, respectively.

V. CONCLUSION

This paper proposes a new GEO SAR constellation and establishes a modified signal model for the following signal characteristics analysis and imaging algorithms development. The proposed GEO SAR in reverse equatorial geosynchronous orbit can solve the problem of long synthetic aperture time accompanying with the traditional GEO SAR. The proposed method for GEO SAR constellation design can realize 24-hour availability of the mid-latitude area. The simulation results show that, the given constellation has relatively shorter synthetic aperture time, azimuth invariance property of received echo, and better consistency of imaging performance. That makes benefits for observation flexibility and efficiency. Moreover, by assuming curvilinear motion with constant acceleration for both satellite and target, the instantaneous two-way slant range can be calculated precisely. By approximating linear slant range variation within transmission and reception process of one pulse, the modulation effects of continuous motion on signal can be achieved analytically. By contrast with the traditional signal model, it has additional two phase terms, which need to be compensated to enhance imaging qualities. The simulation results show that, the modified signal model is more suitable for GEO SAR with large squint angle and large time delay.

REFERENCES

[1] K. Tomiyasu, "Synthetic aperture radar in geosynchronous orbit," in *Proc. Antennas Propag. Soc. Int. Symp.*, Mar. 1978, pp. 42–45.

[2] K. Tomiyasu and J. L. Pacelli, "Synthetic aperture radar imaging from an inclined geosynchronous orbit," *IEEE Trans. Geosci. Remote Sens.*, vol. GRS-21, no. 3, pp. 324–329, Jul. 1983.

[3] J. Zhang, Z. Yu, and P. Xiao, "A novel antenna beam steering strategy for GEO SAR staring observation," in *Proc. IEEE Int. Geosci. Remote Sens. Symp. (IGARSS)*, Jul. 2016, pp. 1106–1109.

[4] D. Bruno, S. E. Hobbs, and G. Ottavianelli, "Geosynchronous synthetic aperture radar: Concept design, properties and possible applications," *Acta Astronautica*, vol. 59, nos. 1–5, pp. 149–156, Jul./Sep. 2006.
[5] S. E. Hobbs and D. Bruno, "Radar imaging from GEO: Challenges and applications," in *Proc. Remote Sens. Photogramm. Soc. Annu. Conf.*, 2007, pp. 1–6.
[6] D. Bruno and S. E. Hobbs, "Radar imaging from geosynchronous orbit: Temporal decorrelation aspects," *IEEE Trans. Geosci. Remote Sens.*, vol. 48, no. 7, pp. 2924–2929, Jul. 2010.
[7] T. Zhang, Z. Ding, W. Tian, T. Zeng, and W. Yin, "A 2-D nonlinear chirp scaling algorithm for high squint GEO SAR imaging based on optimal azimuth polynomial compensation," *IEEE J. Sel. Topics Appl. Earth Observ. Remote Sens.*, vol. 10, no. 12, pp. 5724–5735, Dec. 2017.
[8] F. He, Q. Chen, Z. Dong, G. Jin, and D. Liang, "Modeling and high-precision processing of the azimuth shift variation for spaceborne HRWS SAR," *Sci. China Inf. Sci.*, vol. 56, no. 10, pp. 1–12, 2013.
[9] C. Hu, F. Liu, W. Yang, T. Zeng, and T. Long, "Modification of slant range model and imaging processing in GEO SAR," in *Proc. IEEE Int. Geosci. Remote Sens. Symp. (IGARSS)*, Jul. 2010, pp. 4679–4682.
[10] B. Hu, Y. Jiang, Y. Zhang, and T. S. Yeo, "Accurate slant range model and focusing method in geosynchronous SAR," in *Proc. IEEE Int. Geosci. Remote Sens. Symp. (IGARSS)*, Jul. 2015, pp. 4464–4467.
[11] Z. Ding, W. Yin, T. Zeng, and T. Long, "Radar parameter design for geosynchronous SAR in squint mode and elliptical orbit," *IEEE J. Sel. Topics Appl. Earth Observ. Remote Sens.*, vol. 9, no. 6, pp. 2720–2732, Jun. 2016.
[12] D. Koebel, C. Tobehn, and B. Penné, "OHB platforms for constellation satellites," in *Proc. 5th IAA Symp. Small Satell. Earth Observ.*, Berlin, Germany: German Aerospace Center, Apr. 2005, pp. 1–4.
[13] *Global Earthquake Satellite System: A 20-Year Plan to Enable Earthquake Prediction*, document, NASA and JPL, Pasadena, CA, USA, 2003. [Online]. Available: http://solidearth.jpl.nasa.gov/GESS/3123_GESS_Rep_2003.pdf
[14] Y. Tian, S. Guo, and W. Yu, "'Stop-and-go' error analysis of geosynchronous SAR," *Sci. China Inf. Sci.*, vol. 59, no. 6, 2016, Art. no. 062306.
[15] P. Prats-Iraola, R. Scheiber, M. Rodríguez-Cassolà, S. Wollstadt, J. Mittermayer, B. Bräutigam, M. Schwerdt, A. Reigber, and A. Moreira, "High precision SAR focusing of TerraSAR-X experimental staring spotlight data," in *Proc. IEEE Int. Geosci. Remote Sens. Symp. (IGARSS)*, Jul. 2012, pp. 3576–3579.
[16] Y. Liu, M. Xing, G. Sun, X. Lv, Z. Bao, W. Hong, and Y. Wu, "Echo model analyses and imaging algorithm for high-resolution SAR on high-speed platform," *IEEE Trans. Geosci. Remote Sens.*, vol. 50, no. 3, pp. 933–950, Mar. 2012.
[17] G. Sun, M. Xing, Y. Wang, Y. Liu, Y. Zhang, Y. Wu, and Z. Bao, "A new signal model for a wideband synthetic aperture imaging sensor," *Can. J. Remote Sens.*, vol. 37, no. 2, pp. 171–183, 2011.
[18] H. Kuang, J. Chen, W. Yang, Y.-Q. Zhu, J. Zhou, and C.-S. Li, "Accurate compensation of stop-go approximation for high resolution spaceborne SAR using modified hyperbolic range equation," in *Proc. IEEE Int. Geosci. Remote Sens. Symp. (IGARSS)*, Jul. 2014, pp. 462–465.
[19] L. Huang, C. Ding, H. Zhang, X. Qiu, and B. Han, "A geosynchronous SAR constellation for mid-latitude continuous observation," in *Proc. 12th Eur. Conf. Synth. Aperture Radar (VDE)*, Jun. 2018, pp. 1–4.
[20] S. Hobbs and J. P. Sanchez, "Laplace plane and low inclination geosynchronous radar mission design," *Sci. China Inf. Sci.*, vol. 60, no. 6, Jun. 2017, Art. no. 060305.
[21] S. Hobbs, J. P. Sanchez, C. Convenevole, A. Gibbings, C. Germani, and A. M. Guarnieri, "G-CLASS: A geosynchronous radar mission to study the diurnal water cycle," in *Proc. 69th Int. Astron. Congr. (IAC)*, Bremen, Germany, 2018.
[22] C. Hu, T. Long, T. Zeng, F. Liu, and Z. Liu, "The accurate focusing and resolution analysis method in geosynchronous SAR," *IEEE Trans. Geosci. Remote Sens.*, vol. 49, no. 10, pp. 3548–3563, Oct. 2011.

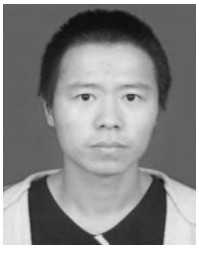

HAILONG XU received the B.S. degree in electronic engineering from Jilin University, Jilin, China, in 2017. He is currently pursuing the M.S. degree with the University of Chinese Academy of Sciences, also with the Key Laboratory of Technology in Geo-Spatial Information Processing and Application System, CAS, and also with the Institute of Electronics, Chinese Academy of Sciences. His research interests include synthetic aperture radar (SAR) signal processing and new systems for SAR imaging.

LIJIA HUANG received the B.S. degree in electronic engineering from Beihang University, Beijing, China, in 2006, and the Ph.D. degree in signal and information processing from the Graduate University of the Chinese Academy of Sciences, Beijing, in 2011. She is currently with the Key Laboratory of Technology in Geo-Spatial Information Processing and Application System, and also with the Institute of Electronics, Chinese Academy of Sciences, Beijing.

XIAOLAN QIU received the B.S. degree in electronic engineering from the University of Science and Technology of China, Hefei, China, in 2004, and the Ph.D. degree in signal and information processing from the Graduate University of the Chinese Academy of Sciences, Beijing, China, in 2009. She is currently with the Key Laboratory of Technology in Geo-Spatial Information Processing and Application System and also with the Institute of Electronics, Chinese Academy of Sciences, Beijing.

BING HAN received the B.S. degree in electronic engineering from Beihang University, Beijing, China, in 2003, and the Ph.D. degree in signal and information processing from the Graduate University of the Chinese Academy of Sciences, Beijing, in 2008. She is currently with the Key Laboratory of Technology in Geo-Spatial Information Processing and Application System and also with the Institute of Electronics, Chinese Academy of Sciences, Beijing.

LIHUA ZHONG received the B.S. degree in electronic engineering from Beihang University, Beijing, China, in 2007, and the Ph.D. degree in signal and information processing from the Graduate University of Chinese Academy of Sciences, Beijing, in 2013. Since 2013, he has been with the Institute of Electronics, Chinese Academy of Sciences, Beijing. His research interests include the processing and radiometric correction algorithms for spaceborne synthetic aperture radar.

DADI MENG received the B.S. degree in communication engineering from Xi'an Jiaotong University, Xi'an, China, in 2001, and the Ph.D. degree in signal and information processing from the Graduate University of Chinese Academy of Sciences, Beijing, China, in 2006. From 2006 to 2008, he was a Research Assistant of geo-spatial information processing and applied system with the Key Laboratory of Technology, Chinese Academy of Sciences, Beijing, and also with the Institute of Electronics, Chinese Academy of Sciences, Beijing. Since 2009, he has been an Associate Research Fellow with the Key Laboratory of Technology. His research interests include airborne synthetic aperture radar (SAR) motion compensation, SAR data processing, and implementation of SAR processing on graphic processor unit.